Interactive Airfoil Calculations with Higher-Order Viscous-Flow Equations

D. W. Zingg* and G. W. Johnston†
University of Toronto Institute for Aerospace Studies, Toronto, Ontario, M3H 5T6 Canada

A critical examination of the use of higher-order viscous-flow equations in the computation of airfoil flowfields with a viscid-inviscid interaction scheme is presented. Comparisons are made between experimental data and interactive solutions obtained using the boundary-layer equations, the second-order boundary-layer equations, and the Navier-Stokes equations, with corresponding approximations to the viscid-inviscid matching conditions, for flows about symmetric and aft-loaded airfoils. In all cases, the viscous solution is coupled with a potential-flow solution. The results are restricted to attached, incompressible flow. An important feature of the comparisons is that the numerical algorithm, computational grid, and turbulence model are the same for all of the computations. Consequently, the effects of the higher-order terms can be studied separately from the influence of these factors. Detailed comparisons of computed and experimental results show that normal pressure gradients can be significant in the shear layers near the airfoil trailing edge and that the boundary-layer equations underestimate the boundary-layer growth in this region. The higher-order terms in the viscous-flow equations do not affect the lift and moment predictions but lead to significantly higher predictions of drag.

Introduction

NUMERICAL algorithms for the computation of viscous flows can be divided into two categories: global procedures that solve viscous equations throughout the domain and interactive procedures that couple separate viscous and inviscid solutions. The interactive approach is usually more efficient but is less general. Typically, the boundary-layer equations are solved in the shear layers. These equations, which are a first-order approximation to the Navier-Stokes equations for high Reynolds number, neglect the normal pressure gradient. However, toward the trailing edge of an airfoil section, where the turbulent boundary layer is thick and the streamline curvature may be high, the normal pressure gradient in the viscous layers can be significant. Consequently, the generality of interactive procedures can be improved by solving higher-order viscous-flow equations in the shear layers.

Accurate calculation of the flow in the trailing-edge region of an airfoil requires the inclusion of higher-order terms in both the viscous-flow equations and the viscid-inviscid matching conditions. In particular, the normal pressure gradient must be represented through some form of the normal-momentum equation. Commonly used higher-order approximations to the Navier-Stokes equations include the thin-layer Navier-Stokes equations, the partially-parabolized Navier-Stokes equations,[1] and the reduced Navier-Stokes equations.[2] All of these approximations neglect streamwise gradients of the viscous and turbulence terms in the Reynolds-averaged Navier-Stokes equations. All inviscid terms are retained. Therefore, the upstream transport of information associated with streamwise diffusion is neglected, but the upstream influence of the pressure field is retained. The first-order boundary-layer equations, being parabolic, neglect all forms of upstream influence other than convection. The second-order boundary-layer equations for laminar flow[3] are also parabolic, whereas the turbulent form[4,5] is parabolic if streamwise gradients of turbulence terms are neglected. The upstream influence associated with convection in reversed-flow regions is not an elliptic effect and is retained in all of the equations.

Received March 1, 1990; presented as Paper 90-1533 at the AIAA 21st Fluid Dynamics, Plasmadynamics and Lasers Conference, Seattle, WA, June 18–20, 1990; revision received and accepted for publication Oct. 22, 1990. Copyright © 1991 by the American Institute of Aeronautics and Astronautics, Inc. All rights reserved.

*Assistant Professor. Member AIAA.
†Professor, 4925 Dufferin St.

There are three primary sources of error in the computation of airfoil flowfields: numerical errors arising from inadequate resolution or unsuitable grids, turbulence modeling errors, and errors arising from the use of approximate forms of the Navier-Stokes equations. Interactive boundary-layer procedures are generally less prone to numerical error than global procedures for the Navier-Stokes equations. Turbulence modeling errors are important in both interactive and global procedures, particularly for separated flows. When numerical solutions are compared with experimental data, which are also subject to error, it can be difficult to distinguish between errors from these various sources. Calculations and measurements of turbulent trailing-edge flows are reported in Refs. 6–10. The measurements confirm the presence of substantial normal pressure gradients on the aft portion of the suction surface and in the near wake of a lifting airfoil, even under unseparated flow conditions. Comparisons of Reynolds-averaged Navier-Stokes solutions with experimental data suggest that accurate representation of the viscid-inviscid interaction is of primary importance for attached flows, whereas detailed turbulence modeling is required for separated flows.

Comprehensive reviews of procedures for the computation of airfoil flowfields, emphasizing viscid-inviscid interaction procedures, can be found in Refs. 11–13. These reviews and the compilations in which they are contained include many examples of viscid-inviscid interaction procedures for calculating separated flows about airfoils. Semi-inverse and quasi-simultaneous coupling procedures are generally used, with the latter being more robust and efficient. Interactive procedures with higher-order viscous-flow equations are presented in Refs. 14–17.

References 18–20 present comparisons between an interactive procedure that couples separate boundary-layer and potential-flow solutions and a global procedure that solves the thin-layer Navier-Stokes equations. The interactive procedure is considerably more accurate than the global procedure. However, the comparisons are inconclusive primarily because the global solutions are grid dependent. A similar comparison is reported in Ref. 21 for a separating trailing-edge flow.

The purpose of the present study is to quantify the effects of normal pressure gradients and other higher-order terms on the calculation of attached, incompressible, turbulent flow about an airfoil and, furthermore, to establish the merits and limitations of the second-order boundary-layer equations in this context. Comparisons are made between experimental data and interactive solutions obtained using the boundary-

layer equations, the second-order boundary-layer equations, and the Navier-Stokes equations, with corresponding approximations to the viscid-inviscid matching conditions. The Navier-Stokes equations are solved using an iterative marching scheme that accounts for the upstream influence of the pressure field only, neglecting the upstream influence due to viscous and turbulent diffusion. In all cases, the viscous solution is coupled with a potential-flow solution. An important feature of the comparisons is that the numerical algorithm, computational grid, and turbulence model are the same for all of the computations. Consequently, the effects of the higher-order terms can be studied separately from the influence of these factors. Further details of the present study can be found in Ref. 22.

Governing Equations

Viscous Flow

This section presents the Navier-Stokes equations and the first- and second-order boundary-layer equations for two-dimensional, steady, incompressible flow. Physical variables are used with an orthogonal, curvilinear, body-fitted coordinate system, in which s is the distance along the surface, the n coordinate lines are straight and normal to the surface, and u and v are the corresponding velocity components. The curvature $\kappa(s)$ is positive for a convex surface and $h = 1 + n\kappa(s)$. Pressure and the fluid density are given by p and ρ, respectively. The kinematic viscosity is given by ν. The primes denote a fluctuating component of velocity, and an overbar denotes a time average. With these definitions, the Reynolds-averaged Navier-Stokes equations are[23]

$$u_s + (hv)_n = 0 \tag{1a}$$

$$uu_s + v(hu)_n + (p_s/\rho) = \nu h\{h^{-1}[(hu)_n - v_s]\}_n - (\overline{u'^2})_s - h(\overline{u'v'})_n - 2\kappa\overline{u'v'} \tag{1b}$$

$$uv_s + hvv_n - \kappa u^2 + (hp_n/\rho) = -\nu h\{h^{-1}[(hu)_n - v_s]\}_s - h(\overline{v'^2})_n - (\overline{u'v'})_s - \kappa(\overline{v'^2} - \overline{u'^2}) \tag{1c}$$

The boundary-layer approximation is based upon an asymptotic expansion of the Navier-Stokes equations for high Reynolds number. The classical (first-order) boundary-layer equations, obtained by retaining terms of relative order unity, are

$$u_s + v_n = 0 \tag{2a}$$

$$uu_s + vu_n + (p_s/\rho) = \nu u_{nn} - (\overline{u'v'})_n \tag{2b}$$

$$p_n = 0 \tag{2c}$$

All curvature terms are seen to be of higher order.

The second-order turbulent boundary-layer equations are

$$u_s + (hv)_n = 0 \tag{3a}$$

$$uu_s + v(hu)_n + (p_s/\rho) = \nu(hu_{nn} + \kappa u_n) - (\overline{u'^2})_s - h(\overline{u'v'})_n - 2\kappa\overline{u'v'} \tag{3b}$$

$$-\kappa u^2 + (p_n/\rho) = -(\overline{v'^2})_n \tag{3c}$$

The second-order normal-momentum equation is valid only for very thin boundary layers in which the streamline curvature is roughly constant. However, its range of validity can be extended by using a representative mean value of the curvature.

Viscid-Inviscid Matching Conditions

In order to account for viscid-inviscid interactions, the inviscid solution must be required to satisfy matching conditions associated with displacement and curvature effects. The displacement effect is associated with the displacement of the inviscid streamlines caused by the boundary layers and wake. In its exact form, the displacement condition requires that the normal velocities given by the viscous and inviscid solutions must be equal at the edge of the boundary layer, i.e.,

$$v_{ie} = v_e \tag{4}$$

where the subscript i denotes the inviscid solution and the subscript e denotes the boundary-layer edge, defined by $n = \delta(s)$. The location of the boundary-layer edge is determined by the viscous solution procedure using a criterion based on the velocity gradient.[22]

The displacement effect can be incorporated through either the solid-body model or the transpiration model. Only the latter model is presented here. In the transpiration model, the inviscid solution is continued to the body, and the matching condition is applied at the surface. The continuation of the inviscid solution into the viscous region is referred to as the equivalent inviscid flow. The generalized displacement thickness is defined as[13]

$$\delta^* = \frac{1}{u_e}\int_0^\delta (u_i - u)\, dn \tag{5}$$

In order to satisfy Eq. (4), the equivalent inviscid flow must satisfy the following surface boundary condition:

$$v_{i0} = \frac{d}{ds}(u_e\delta^*) \tag{6}$$

where the subscript 0 denotes the surface of the body. The first-order approximation to the generalized displacement thickness is found by assuming that the streamwise velocity given by the equivalent inviscid solution is constant in the boundary layer. With this assumption, Eq. (5) becomes

$$\delta_1^* = \int_0^\delta \left(1 - \frac{u}{u_e}\right) dn \tag{7}$$

A second-order definition of the displacement thickness can be derived by assuming a linear variation of u_i in the boundary layer. Expanding u_i as a Taylor series about the boundary-layer edge gives

$$u_i = u_e - \frac{\partial u_i}{\partial n}\Big|^{n=\delta}(\delta - n) + O(\delta^2) \tag{8}$$

In irrotational flow, the normal gradient of u_i can be related to the streamline curvature by the following expression:

$$\kappa_{ie} = -\frac{1}{u_e}\frac{\partial u_i}{\partial n}\Big|^{n=\delta} \tag{9}$$

Substituting Eqs. (8) and (9) into Eq. (5) gives the following expression for the second-order displacement thickness:

$$\delta_2^* = \delta_1^* + (\kappa_{ie}\delta^2/2) \tag{10}$$

This form of the second-order displacement thickness is not unique; a slightly different form is given by Lock.[13] In both cases, the inviscid streamline curvature is treated as constant in the boundary layer. Analogous to the second-order normal-momentum equation, improved accuracy can be obtained in

regions where the curvature varies within the boundary layer by using a representative mean value of the normal gradient of u_i.

The wake curvature effect arises because the normal pressure gradients in the viscous solution in a curved wake are lower than those in the equivalent inviscid solution. In order that the pressure change across the wake in the equivalent inviscid solution be equal to that in the viscous solution, a discontinuity is required in the equivalent inviscid pressure. When normal pressure gradient terms are retained in the viscous equations, the pressure change across the wake can be determined directly from the viscous calculation, and hence the required discontinuity in the equivalent inviscid pressure can be found. When the first-order boundary-layer equations are used, the discontinuity in the equivalent inviscid pressure can be approximated by assuming that the streamline curvature is constant in the wake. With this assumption, the required discontinuity in the equivalent inviscid pressure Δp_i can be determined by integrating the normal momentum equation across the wake, giving

$$\Delta p_i = -\kappa \rho u_w^2 (\delta_{1w}^* + \theta_w) \tag{11}$$

where θ is the momentum thickness, the subscript w indicates the wake, and u_w is the mean of the streamwise velocities at the upper and lower edges of the wake. An alternative procedure is to split the wake into upper and lower portions. The discontinuity in the equivalent inviscid pressure can then be determined such that the inviscid pressure a distance $(\delta_1^* + \theta)_u$ above the wake centerline is equal to the inviscid pressure a distance $(\delta_1^* + \theta)_l$ below the wake centerline, where the subscripts u and l denote the upper and lower portions of the wake, respectively. With the assumption of constant curvature, this condition is equivalent to Eq. (11) to first order. The Kutta condition is enforced by applying the wake curvature condition at the trailing edge.

Numerical Formulation

Viscous Flow

The viscous continuity and streamwise-momentum equations are solved using Keller's box method.[24] The first-order boundary-layer calculation requires a single sweep only, with $p(s,n) = p_e(s)$. When the second-order boundary-layer and Navier-Stokes equations are solved, the box method is used within an iterative procedure to include the pressure calculated from the normal-momentum equation. The Cebeci-Smith algebraic turbulence model[24] is used to determine the Reynolds shear stress. The normal stresses are calculated as empirical multiples of the shear stress, as follows:

$$\overline{u'^2} = 3.5 \mid \overline{u'v'} \mid, \qquad \overline{v'^2} = 2.0 \mid \overline{u'v'} \mid \tag{12}$$

The box method is also used for the turbulent wake calculation. The wake turbulence model given in Ref. 25 is used to calculate the turbulent stresses in the wake.

The iterative procedure for the second-order boundary-layer and Navier-Stokes equations proceeds as follows:

1) The continuity and streamwise-momentum equations are solved simultaneously at each streamwise station with $p(s,n)$ known from the previous iteration.

2) Using the resulting velocity profiles, the pressure is determined by numerically integrating the normal-momentum equation.

The second-order boundary layer equations require one such iteration per viscid-inviscid iteration. When the Navier-Stokes equations are solved, three viscous iterations are performed per viscid-inviscid iteration. Three iterations are used because under relaxation is required for stability near the trailing edge. In both cases, the pressure field is stored. Since a marching procedure is used, the upstream influence associated with streamwise stress gradients is neglected, although the streamwise stress gradient terms are retained. The upstream influence of the pressure field is retained in the Navier-Stokes calculation because centered differences are used for the streamwise derivatives in the normal-momentum equation. Therefore, the calculation of the pressure from the normal-momentum equation at a given streamwise station requires velocity and turbulence profiles from the next downstream station, and hence the upstream influence of the pressure field travels at the rate of one streamwise step per iteration. In the second-order normal-momentum equation, there are no streamwise derivatives and thus the second-order boundary-layer equations permit no upstream influence from the pressure field.

Toward the trailing edge, the streamline curvature associated with the rapid thickening of the boundary layer is large, and therefore the surface curvature is not representative of the mean streamline curvature in the boundary layer. The present second-order calculations use the inviscid streamline curvature at the shear-layer edge, determined from Eq. (9), in the normal-momentum equation. This results in a good approximation to the pressure change in the shear layer because the deviation of the curvature from the value at the edge is largest near the surface, where the velocity is small. The use of the curvature at the edge of the shear layer also provides continuity in the normal pressure gradient between the viscous and inviscid solutions. Near a trailing edge with a finite wedge angle, this value of streamline curvature leads to an underestimate of the pressure change through the shear layer, since the streamline curvature tends to infinity at the surface. An improved approximation can be obtained by prescribing the variation in the curvature in the shear layer at the trailing edge based on the variation of the curvature of potential-flow streamlines near a corner, as follows[22]:

$$\kappa = \kappa_{ie}/(n/\delta) \tag{13}$$

Viscid-Inviscid Matching

Since the present procedures are restricted to attached flow, the direct approach to viscid-inviscid matching is used. The viscous and inviscid calculations are repeated iteratively until a self-consistent solution is obtained. Since the steady incompressible potential-flow equations are elliptic, the viscid-inviscid iterations provide an additional mechanism for viscous upstream influence. The inviscid solution is found using the panel method of Ref. 26. On the airfoil, the displacement-effect matching condition determines the inner boundary condition for the inviscid solution. In the wake, the required discontinuity in the inviscid normal velocity associated with the displacement effect is provided by a line of sources located on the trailing-edge streamline. Similarly, the discontinuity in the inviscid pressure associated with the wake curvature effect is provided by a line of vortices.

The second-order approximation to the displacement thickness is given by Eq. (10), with the inviscid streamline curvature at the boundary-layer edge replaced by a representative mean value, found from the following expression:

$$\overline{\kappa_i} = -\frac{1}{u_e}\overline{\frac{\partial u_i}{\partial n}} \tag{14}$$

The mean value of the normal gradient of the inviscid streamwise velocity is given by

$$\overline{\frac{\partial u_i}{\partial n}} = \frac{u_e - u_i^{n=n_1}}{\delta - n_1} \tag{15}$$

where $n_1 = 0.25\ \delta$. The use of such a representative mean curvature in the expression for the second-order displacement thickness provides a more accurate approximation to the generalized displacement thickness than that obtained using the

inviscid curvature at the boundary-layer edge.[22] When the Navier-Stokes equations are solved in the shear layers, the exact form of the displacement effect condition, Eq. (4), is used.

The wake curvature condition requires that

$$p_{0u} = p_{0l} \tag{16}$$

where p_{0u} is the pressure at the trailing-edge streamline calculated by integrating the normal-momentum equation from the upper edge of the wake, and p_{0l} is calculated by integrating from the lower edge. When the first-order boundary equations are solved, p_{0u} and p_{0l} are determined as follows:

$$p_{0u} = p_i^{n=(\delta_1^*+\theta)u}, \qquad p_{0l} = p_i^{n=(\delta_1^*+\theta)l} \tag{17}$$

Similarly, the pressure at the surface is determined from the equivalent inviscid pressure calculated a distance $(\delta_1^* + \theta)$ from the surface when the first-order boundary-layer equations are solved. This pressure and the corresponding inviscid velocity provide the outer boundary conditions for the first-order viscous calculation. When the higher-order viscous equations are solved, the pressure at the surface is determined directly from the normal-momentum equation. The edge velocity and pressure used in the higher-order viscous calculations are determined from the inviscid solution at $n = \delta$.

Results and Discussion

In this section, computational and experimental results are compared for a symmetric airfoil section and an aft-loaded airfoil section. The symmetric airfoil studied is the RAE 101 section,[27] which has a thickness-to-chord ratio of 10%. The data presented for this airfoil were obtained at a chord Reynolds number of 1.6×10^6 and a freestream Mach number of less than 0.20. The aft-loaded airfoil studied is the NLF(1)-0416 section,[28] which has a thickness-to-chord ratio of 16%. The data for this airfoil were obtained at a chord Reynolds number of 4.0×10^6 and a freestream Mach number of 0.10. Standard wind-tunnel corrections have been applied to the experimental data in both cases. The highest local value of Mach number in the cases studied is roughly 0.35, and thus compressibility effects are likely to be smaller than the experimental error. For the computations on the symmetric airfoil, the location of the onset of boundary-layer transition was determined such that the calculated and experimental values of momentum thickness agree a short distance downstream of the transition region. On the aft-loaded airfoil, measured transition-point locations were used.

Computational results from four procedures are presented. The first- and second-order procedures solve the first- and second-order boundary-layer equations, together with the first- and second-order approximations to the displacement effect, respectively. The modified second-order procedure solves the second-order boundary-layer equations using the prescribed variation in the streamline curvature at the trailing edge, given by Eq. (13), in the normal-momentum equation, together with the second-order approximation to the displacement effect. The Navier-Stokes procedure solves the Navier-Stokes equations and uses the exact form of the displacement effect matching condition. All of the procedures use the same computational grid. The normal grid spacing nearest the surface in the turbulent viscous calculation is equal to 1×10^{-5} chords. The ratio of adjacent grid spacings is equal to 1.14; consequently, 40 to 50 points are required in the boundary layer at each streamwise station.

The computed variation of the pressure coefficient in the boundary layer on the upper surface of the aft-loaded airfoil at $x/c = 0.98686$ is shown in Fig. 1. The pressure coefficient, C_p, is defined as $C_p = 2(p - p_\infty)/\rho_\infty U_\infty^2$, x is the Cartesian coordinate parallel to the airfoil chord, c is the airfoil chord length, U_∞ is the freestream speed, and α is the angle of attack. The computed results agree qualitatively with the measurements of Nakayama.[10] The second-order results are similar to the Navier-Stokes results, indicating that the streamline curvature is roughly constant through most of the boundary layer at this station. The sign of the normal pressure gradient corresponds to concave streamline curvature, which occurs as a result of the rapid thickening of the suction-surface boundary layer near the trailing edge.

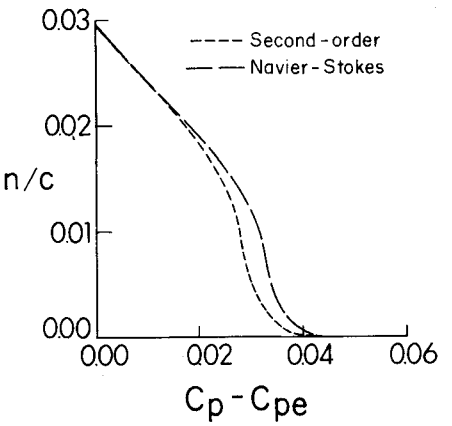

Fig. 1 Computed pressure variation in the boundary layer on the upper surface of the NLF(1)-0416 airfoil at $x/c = 0.98686$ with $\alpha = 0.01$ deg.

Figures 2a and 2b compare the computed and measured variation in pressure in the boundary layers at the trailing edge of the symmetric airfoil. The apparent discontinuity at $n = 0$ in Fig. 2b arises because the difference between the local pressure coefficient, C_p, and the edge pressure coefficient, C_{pe}, is plotted. Thus, the difference shown at $n = 0$ is equal to the difference in the pressure coefficients at the upper and lower boundary-layer edges. The normal pressure gradients correspond to concave streamline curvature due to the finite trailing-edge angle. The second-order procedure underestimates the normal pressure gradients near the surface at the trailing edge relative to both the experimental data and the Navier-Stokes predictions, indicating that the streamline curvature increases toward the surface. The modified second-order procedure shows much better agreement with the experimental data, providing some confirmation of the applicability of Eq. (13).

The computed pressure variation in the boundary layers at the trailing edge of the aft-loaded airfoil is shown in Figs. 3a and 3b. The modified second-order procedure predicts boundary-layer separation at the trailing edge and hence is not shown. The normal pressure gradient on the lower surface of the aft-loaded airfoil corresponds to convex streamline curvature, in contrast to that on the symmetric airfoil. This agrees with the experimental data of Nakayama,[10] who studied an airfoil with little aft-loading and an airfoil with substantial aft-loading, showing precisely the same trend. The difference in the pressure coefficients at the upper and lower boundary-layer edges, shown as the difference at $n = 0$ in the figures, is much larger on the aft-loaded airfoil. The second-order predictions for the aft-loaded airfoil display better agreement with the Navier-Stokes predictions than those for the symmetric airfoil, probably because the aft-loaded airfoil has a smaller trailing-edge angle.

The computed boundary-layer characteristics on the upper surface of the symmetric airfoil at an angle of attack of 4.09 deg are compared to the experimental values in Fig. 4. All of the procedures underestimate both the displacement thickness and the momentum thickness at the trailing edge. The difference between computation and experiment in the prediction of the boundary-layer characteristics at the trailing edge is substantially reduced when the higher-order procedures are used. The computed boundary-layer characteristics

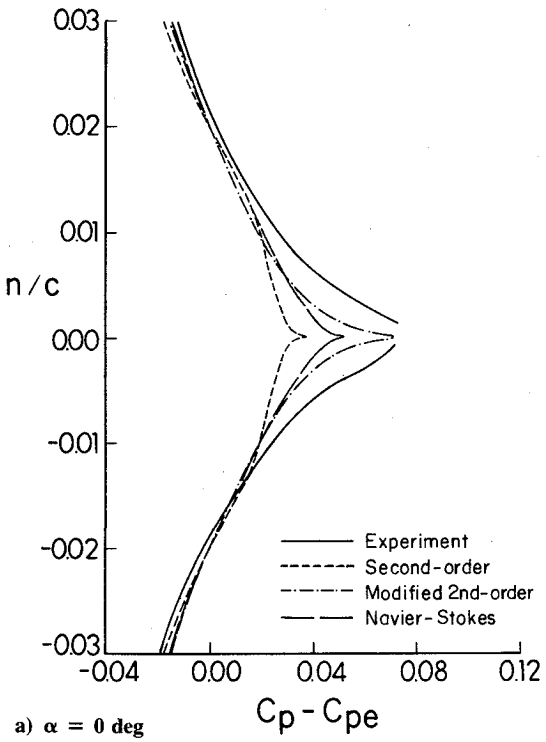

a) α = 0 deg

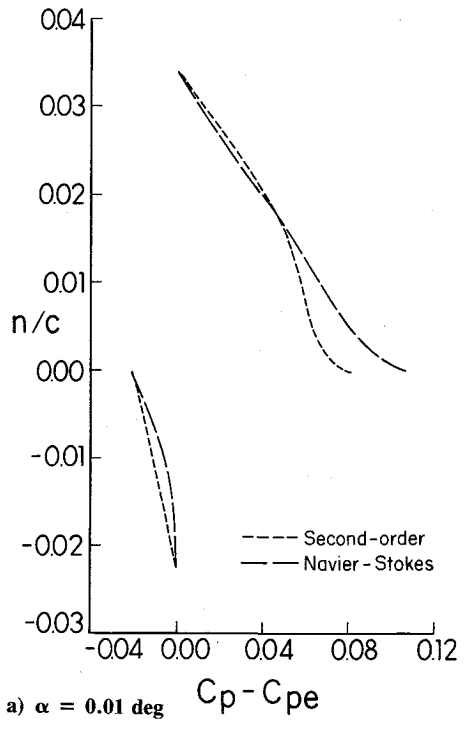

a) α = 0.01 deg

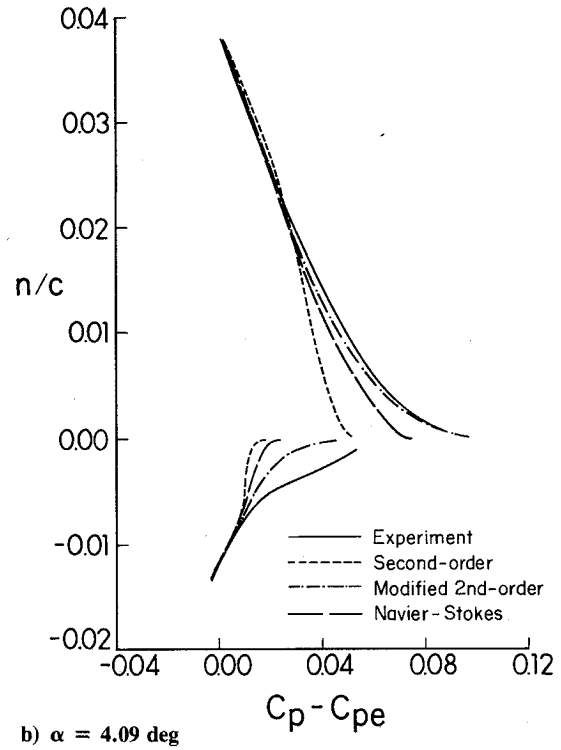

b) α = 4.09 deg

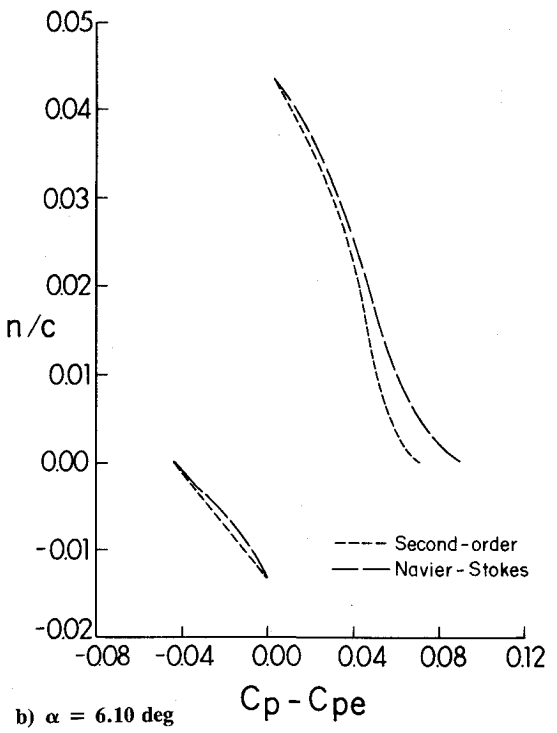

b) α = 6.10 deg

Fig. 2 Computed and experimental pressure variation in the boundary layers at the trailing edge of the RAE 101 airfoil.

Fig. 3 Computed pressure variation in the boundary layers at the trailing edge of the NLF(1)-0416 airfoil.

on the aft-loaded airfoil at an angle of attack of 0.01 deg are shown in Figs. 5 and 6. On the upper surface, the results agree qualitatively with those for the symmetric airfoil. On the lower surface, the results are somewhat different. The lower surface of the airfoil has concave curvature on the last 20% of the chord. At the trailing edge, the streamlines are convex, as shown by Fig. 3. Therefore, the higher-order procedures predict values of displacement and momentum thickness which are higher than the first-order predictions as the trailing edge is approached, but they predict lower values right at the trailing edge.

Computed pressure distributions for the symmetric section are compared with experiment in Figs. 7a and 7b. The pressure distributions computed using the Navier-Stokes procedure are shown; the results of the other procedures are virtually indistinguishable. The agreement with the experimental

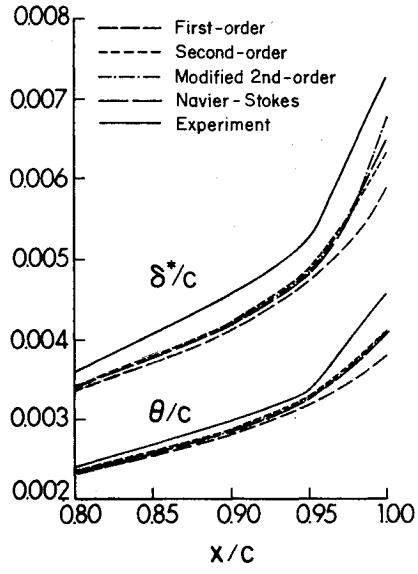

Fig. 4 Computed and experimental displacement and momentum thickness distributions on the upper surface of the RAE 101 airfoil at $\alpha = 4.09$ deg.

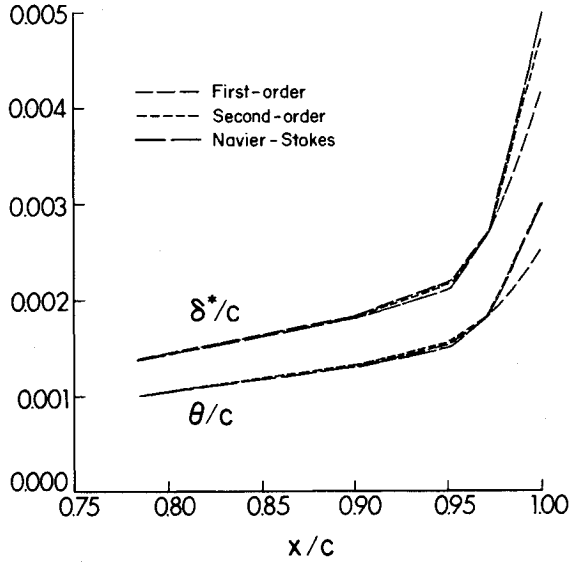

Fig. 5 Computed displacement and momentum thickness distributions on the upper surface of the NLF(1)-0416 airfoil at $\alpha = 0.01$ deg.

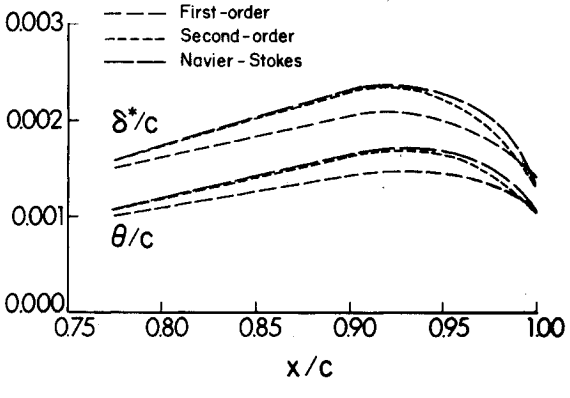

Fig. 6 Computed displacement and momentum thickness distributions on the lower surface of the NLF(1)-0416 airfoil at $\alpha = 0.01$ deg.

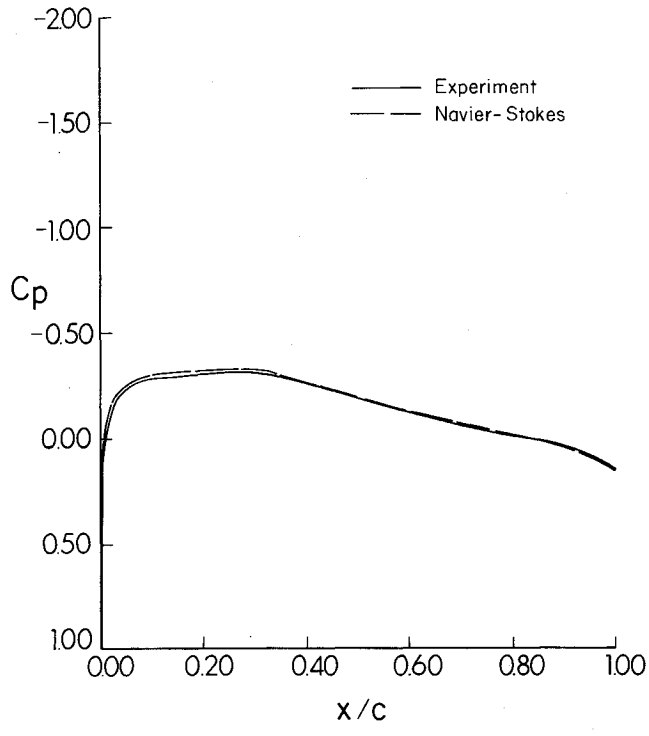

a) $\alpha = 0$ deg

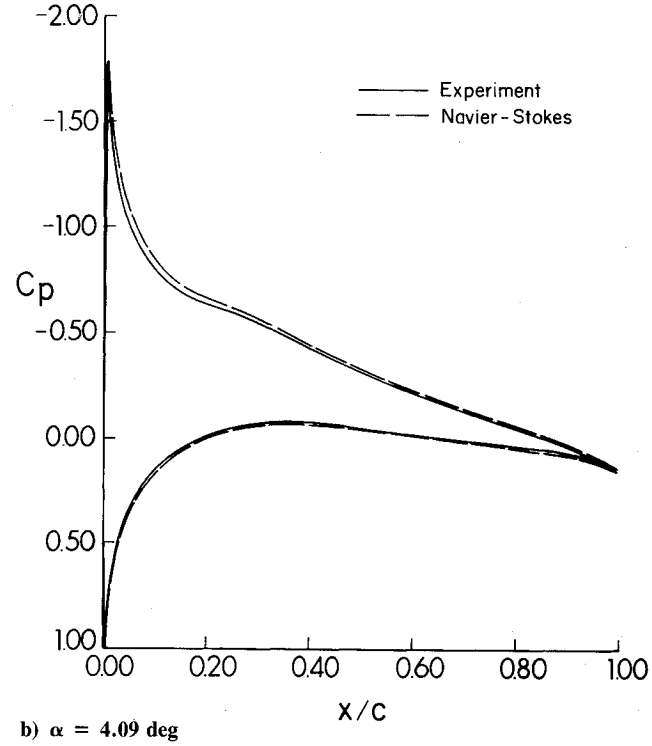

b) $\alpha = 4.09$ deg

Fig. 7 Computed and experimental pressure distributions on the RAE 101 airfoil.

data is very good. Even though the first-order procedure underestimates the displacement thickness on the suction surface near the trailing edge, relative to the higher-order procedures, all of the procedures produce very similar pressure distributions for both airfoils. This occurs because the first-order approximation to the displacement thickness overestimates the displacement thickness when the streamlines are concave. Therefore, the error in the viscous calculation due to the first-order approximation is cancelled to a large extent

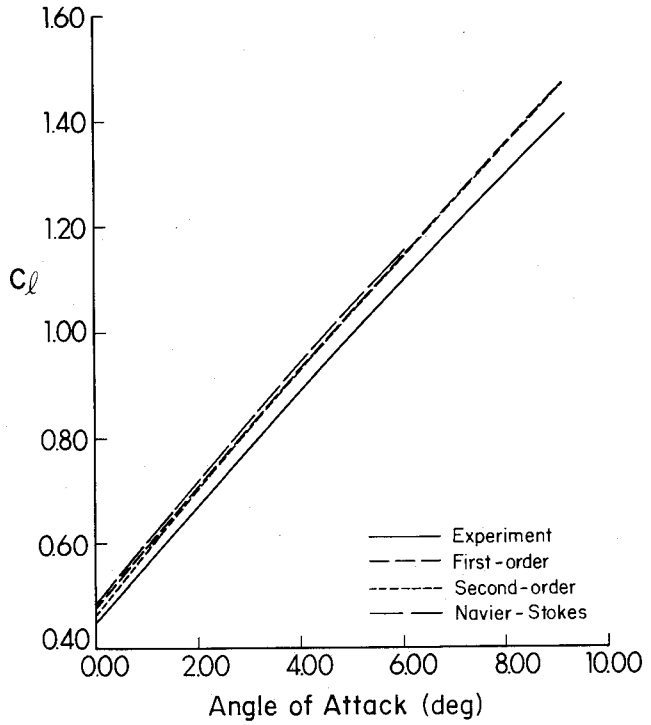

a) Lift coefficient

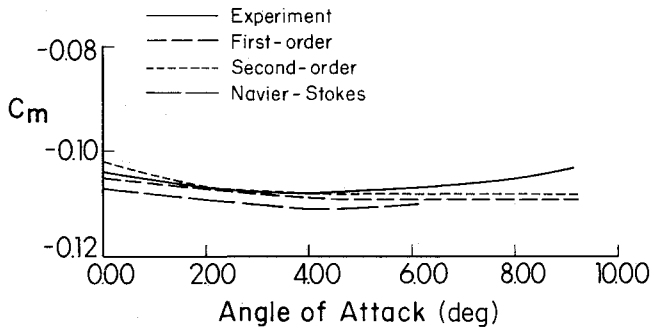

b) Moment coefficient

Fig. 8 Computed and experimental lift and moment coefficients for the NLF(1)-0416 airfoil.

by the error associated with the first-order matching condition.

The computed lift and pitching moment coefficients for the aft-loaded airfoil are compared to the experimental data in Figs. 8a and 8b. No results are shown for the Navier-Stokes procedure at angles of attack above 6.10 deg, since boundary-layer separation is predicted. The three procedures produce roughly equal predictions of lift and moment coefficients. The computed moment coefficients agree well with the experimental data, but the lift coefficients are overestimated. The slope of the lift curve is well predicted, however, which suggests that the experimental values of angle of attack could be in error.

Figure 9 shows the drag coefficients computed for the aft-loaded airfoil, in comparison with the experimental data. The drag coefficients are computed by applying the Squire-Young formula[15] at a wake station 20% of the chord aft of the trailing edge. This station lies sufficiently far aft of the trailing edge that higher-order terms are negligible. Furthermore, at this station, the wake shape factor is less than 1.3 in all of the cases studied. Therefore, virtually no error is introduced by the empirical relation between the edge velocity and the wake shape factor upon which the Squire-Young formula is based.[15] The computed drag coefficients are too low, particularly when

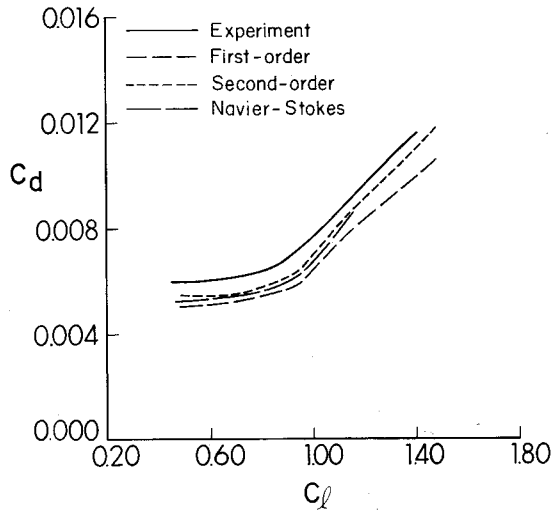

Fig. 9 Computed and experimental drag polars for the NLF(1)-0416 airfoil.

the first-order procedure is used. The drag coefficients computed using the higher-order procedures show better agreement with the experiment, especially at high angles of attack. The drag coefficients computed using the second-order procedure show good agreement with those computed using the Navier-Stokes procedure.

Conclusions

A critical examination of the use of higher-order viscous-flow equations in the computation of airfoil flowfields with a viscid-inviscid interaction scheme has been presented. Comparisons were made between experimental data and solutions obtained by solving the boundary-layer equations, the second-order boundary-layer equations, and the Navier-Stokes equations, with corresponding approximations to the viscid-inviscid matching conditions, for flows about symmetric and aft-loaded airfoils. The results are restricted to attached, incompressible flow. An important feature of the comparisons is that the numerical algorithm, computational grid, and turbulence model were the same for all of the computations. Consequently, the effects of the higher-order terms can be studied separately from the influence of these factors.

The normal pressure gradients predicted by the higher-order procedures are significant in the trailing-edge region of both airfoils. Thus, the higher-order terms have a significant effect on the boundary-layer and wake characteristics near the trailing edge. The first-order procedure underestimates the boundary-layer displacement and momentum thicknesses on the upper surface near the trailing edge, relative to the higher-order procedures. The higher-order terms do not significantly affect lift and moment predictions but lead to higher and more accurate predictions of drag. The drag coefficients computed using the second-order procedure show good agreement with the predictions of the Navier-Stokes procedure. A modified second-order procedure has also been developed in which the variation of the streamline curvature in the boundary layer at the trailing edge is prescribed. Although this procedure produces excellent agreement with experiment in the variation of pressure in the boundary layers at the trailing edge, it appears to predict boundary-layer separation prematurely.

References

[1]Anderson, D. A., Tannehill, J. C., and Pletcher, R. H., *Computational Fluid Mechanics and Heat Transfer*, Hemisphere, New York, 1984.

[2]Himansu, A., and Rubin, S. G., "Multigrid Acceleration of a Relaxation Procedure for the Reduced Navier-Stokes Equations," *AIAA Journal*, Vol. 26, No. 9, 1988, pp. 1044–1051.

[3]Van Dyke, M., "Higher-Order Boundary-Layer Theory," *Annual Review of Fluid Mechanics*, Vol. 1, 1969, pp. 265–292.

[4]Cebeci, T., Hirsh, R. S., and Whitelaw, J. H., "On the Calculation of Laminar and Turbulent Boundary Layers on Longitudinally Curved Surfaces," *AIAA Journal*, Vol. 17, No. 4, 1979, pp. 434–436.

[5]Eghlima, A., and Kleinstreuer, C., "Numerical Anaysis of Attached Turbulent Boundary Layers Along Strongly Curved Surfaces," *AIAA Journal*, Vol. 23, No. 2, 1985, pp. 177–184.

[6]Baker, A. J., Yu, J. C., Gatski, T. B., and Orzechowski, J. A., "Prediction and Measurement of Turbulent Trailing Edge Flows," AIAA Paper 80-1395, 1980.

[7]Viswanath, P. R., Cleary, J. W., Seegmiller, H. L., and Horstmann, C. C., "Trailing-Edge Flows at High Reynolds Number," AIAA Paper 79-1503, 1979.

[8]Horstmann, C. C., "Numerical Simulation of Turbulent Trailing Edge Flows," *Numerical and Physical Aspects of Aerodynamic Flows II*, edited by T. Cebeci, Springer-Verlag, New York, 1984, pp. 112–124.

[9]Nakayama, A., "Characteristics of the Flow Around Conventional and Supercritical Airfoils," *Journal of Fluid Mechanics*, Vol. 160, 1985, pp. 155–179.

[10]Nakayama, A., "Measurements of Attached and Separated Turbulent Flows in the Trailing Edge Regions of Airfoils," *Numerical and Physical Aspects of Aerodynamic Flows II*, edited by T. Cebeci, Springer-Verlag, New York, 1984, pp. 233–255.

[11]Cebeci, T., Stewartson, K., and Whitelaw, J. H., "The Calculation of Two-Dimensional Flow Past Airfoils," *Numerical and Physical Aspects of Aerodynamic Flows II*, edited by T. Cebeci, Springer-Verlag, New York, 1984, pp. 1–40.

[12]Cebeci, T., and Whitelaw, J. H., "Calculation methods for Aerodynamic Flows—A Review," *Numerical and Physical Aspects of Aerodynamic Flows III*, edited by T. Cebeci, Springer-Verlag, New York, 1986, pp. 1–22.

[13]Lock, R. C., "A Review of Methods for Predicting Viscous Effects on Aerofoils and Wings at Transonic Speeds," *Computation of Viscid-Inviscid Interactions*, AGARD CP 291, 1981.

[14]Melnik, R. E., "Turbulent Interactions on Airfoils at Transonic Speeds—Recent Developments," *Computation of Viscid-Inviscid Interactions*, AGARD CP 291, 1981.

[15]Lock, R. C., "Prediction of the Drag of Wings at Subsonic Speeds by Viscous/Inviscid Interaction Techniques," AGARD R 723, 1985.

[16]Bradshaw, P., Kavanagh, M. A., and Mobbs, D., "Viscous-Inviscid Matching Using Imbedded Navier-Stokes Solutions," *Numerical and Physical Aspects of Aerodynamic Flows II*, edited by T. Cebeci, Springer-Verlag, New York, 1984, pp. 125–138.

[17]Stern, F., Yoo, S. Y., and Patel, V. C., "Interactive and Large-Domain Solutions of Higher-Order Viscous-Flow Equations," *AIAA Journal*, Vol. 26, No. 9, 1988, pp. 1052–1060.

[18]Mehta, U., Chang, K. C., and Cebeci, T., "A Comparison of Interactive Boundary-Layer and Thin-Layer Navier-Stokes Procedures," *Numerical and Physical Aspects of Aerodynamic Flows III*, edited by T. Cebeci, Springer-Verlag, New York, 1986, pp. 198–215.

[19]Mehta, U., Chang, K. C., and Cebeci, T., "Relative Advantages of Thin-Layer Navier-Stokes and Interactive Boundary-Layer Procedures," NASA TM-86778, 1985.

[20]Chang, K. C., Alemdaroglu, N., Mehta, U., and Cebeci, T., "Further Comparisons of Interactive Boundary-Layer and Thin-Layer Navier-Stokes Procedures," *AIAA Journal*, Vol. 25, No. 10, 1988, pp. 897–903.

[21]Adair, D., Thompson, B. E., Whitelaw, J. H., and Williams, B. R., "Comparison of Interactive and Navier-Stokes Calculations of Separating Boundary-Layer Flows," *Numerical and Physical Aspects of Aerodynamic Flows III*, edited by T. Cebeci, Springer-Verlag, New York, 1986, pp. 168–183.

[22]Zingg, D. W., "Higher-Order Approximations in Interactive Airfoil Calculations," Univ. of Toronto Inst. for Aerospace Studies, Rept. 326, Downsview, Ontario Canada, 1988.

[23]Bradshaw, P., "Effects of Streamline Curvature on Turbulent Flow," AGARD AG-169, 1973.

[24]Cebeci, T., and Bradshaw, P., *Momentum Transfer in Boundary Layers*, Hemisphere, New York, 1977.

[25]Chang, K. C., Bui, M. N., Cebeci, T., and Whitelaw, J. H., "The Calculation of Turbulent Wakes," *AIAA Journal*, Vol. 24, No. 2, pp. 200, 201.

[26]Bristow, D. R., "Development of Panel Methods for Subsonic Analysis and Design," NASA CR 3234, 1980.

[27]Brebner, G. G., and Bagley, J. A., "Pressure and Boundary-Layer Measurements on a Two-Dimensional Wing at Low Speed," RAE R&M No. 2886, Farnborough, 1952.

[28]Somers, D., "Design and Experimental Results for a Natural-Laminar-Flow Airfoil for General Aviation Applications," NASA TP 1861, 1981.